KeAi
CHINESE ROOTS
GLOBAL IMPACT

Available online at www.sciencedirect.com

ScienceDirect

Advances in Climate Change Research 12 (2021) 299–312

www.keaipublishing.com/en/journals/accr/

The presence and influence of glacier surging around the Geladandong ice caps, North East Tibetan Plateau

Owen KING[a,*], Atanu BHATTACHARYA[a,b], Tobias BOLCH[a]

[a] *Department of Geography and Sustainable Development, University of St Andrews, St Andrews, KY16 9AL, UK*
[b] *Department of Remote Sensing and GIS, JIS University, Kolkata, 700109, India*

Received 16 December 2020; revised 22 February 2021; accepted 6 May 2021
Available online 15 May 2021

Abstract

Many glaciers and ice caps on the Tibetan Plateau have retreated and lost mass in recent years in response to temperature increases, providing clear evidence of the impact of climate change on the region. There is increasing evidence that many of the glaciers on the Tibetan Plateau have also shown periodically dynamic behaviour in the form of glacier surging and some even catastrophic collapse events. In this study, we examine the prevalence of glacier surging at the Geladandong ice caps, North East Tibetan Plateau, to better understand the role of surge events in the evolution of glacier mass loss budgets. Using glacier surface elevation change data over the period 1969–2018 and glacier surface velocity data from the ITS_LIVE dataset, we find that 19 outlet glaciers of the ice caps are of surge-type. Our multi-temporal measurements of glacier mass balance show that surge-type glacier mass budgets vary depending on the portion of the surge-cycle captured by geodetic data. At the regional level, pre- and post-surge glacier mass loss variability does not bias regional mass budget estimates, but enhanced, or suppressed, mass loss estimates are likely when small groups of glaciers are examined. Our results emphasise the importance of accurate surge-type glacier inventories and the need to maximise geodetic data coverage over glacierised regions known to contain surge-type glaciers.

Keywords: Glacier surge; Remote sensing; Corona KH-4; Glacier mass balance; ASTER; Tibetan Plateau; Glacier velocity

1. Introduction

The behaviour of glaciers on the Tibetan Plateau provides a clear indication of the impact of climate change on this remote region, the majority of which has an average altitude of more than 5000 m (Shi et al., 1980; Sakai et al., 2015). Glacier behaviour on the Tibetan Plateau is influenced by mid-latitude westerlies, the Indian monsoon and East Asian monsoon and their mass budget has varied heterogeneously over the past few decades (Yao et al., 2012; Mölg et al., 2014; Sakai and Fujita, 2017; Bolch et al., 2019; Shean et al., 2020). Glaciers of the western Tibetan Plateau, in sub-regions such as the Western Kunlun Shan, have shown balanced mass budgets since the 1970s, as have glaciers on the plateaus northern edge (Altun Shan) (Zhou et al., 2018; Bolch et al., 2019); both of these regions are within reach of mid-latitude westerlies, which deliver substantial amounts of winter accumulation. Along the plateaus southern edge (Gandise mountains), in central areas such as the western Nyainqentanghla and in the north east of the region, glacier retreat and mass loss have predominated recently (Yao et al., 2012; Bolch et al., 2019; Shean et al., 2020). Glacier recession in this region impacts local communities through the fluctuation of seasonal and longer term meltwater availability and through the prevalence of glacier hazards such as glacial lake outburst floods (GLOFs) (Allen et al., 2019).

Glaciers on the Tibetan Plateau have been studied in broad scale remote sensing studies (Brun et al., 2017; Shean et al., 2020; Neckel et al., 2014) and at a detailed, localised level

* Corresponding author.
E-mail address: ogak1@st-andrews.ac.uk (KING O.).
Peer review under responsibility of National Climate Center (China Meteorological Administration).

https://doi.org/10.1016/j.accre.2021.05.001

(e.g. Jenkins et al., 2016; Zhang et al., 2016; Liu et al., 2019) but relatively few studies have bridged the gap to study sub-regional glacier variability and the factors driving change over multiple periods. Such studies are important because of the potential for regional level sampling to mask spatial variability in glacier behaviour and its associated drivers (e.g. Brun et al., 2019; King et al., 2019). Recent studies also highlight the dynamic behaviour of Tibetan Plateau glaciers and their ability to react catastrophically to the changing climate in the region (Kääb et al., 2018). Surge-type glacier behaviour has now been documented in several Tibetan Plateau ice caps (e.g. Wu et al., 2018; Zhang et al., 2018; Zhou et al., 2018; Jiang et al., 2012; Liu et al., 2019; Zhang et al., 2020) beyond those documented by Sevestre and Benn (2015). The Aru glacier collapses also emphasises the need for more focussed assessments of Tibetan Plateau glacier change (Kääb et al., 2018).

Here, we assess the evolution of glaciers of the Geladandong ice caps in the Tanggula Shan region of the central Tibetan Plateau. The Geladandong ice caps are located at the western end of the Tanggula mountains; an important climatic divide on the plateau (Fig. 1). The southern slopes of the Tanggula mountains receive the majority of their precipitation from the Indian Monsoon, whereas their northern slopes receive precipitation from continental air masses (Chen et al., 2017). Akin to several other large ice caps found in the central Tibetan Plateau and its northern and eastern periphery, the glaciers of the Geladandong ice caps are predominantly devoid of debris cover and have seen steady glacier area reductions in recent years (Yao et al., 2012) in response to sustained temperature increases (Chen et al., 2017). Geodetic studies (Shean et al., 2020; Brun et al., 2017) show that the broader region has experienced ice mass losses since the millennium. On a more localised scale, Chen et al. (2017) quantified the mass balance of the western Geladandong ice cap and showed modest (-0.21 ± 0.16 m w.e. per year) mass loss between the 1960s and 2000, which increased (-0.33 ± 0.38 m w.e. per year) between 2000 and 2015. Similarly, Zhou et al. (2018) quantified the mass loss rate of the larger, eastern ice cap (Fig. 2) and measured similar mass loss between 1976 and 2000 (-0.22 ± 0.12 m w.e. per year). Several studies have made note of the presence of surge-type glaciers in the area (Chen et al., 2017; Zhou et al., 2018; Xu et al., 2018) but no comprehensive inventory has examined their prevalence in space or time. At the regional scale and over decadal time periods, surge-type glacier mass balance has commonly been found to be comparable to that of non-surge-type glaciers (Bolch et al., 2017; Berthier and Brun, 2019; Lv et al., 2019). However, over shorter time periods, and at the glacier scale, distinct variability in glacier mass loss rates have been noted for surge-type glaciers (Sund et al., 2009; Yde and Knudsen, 2007;

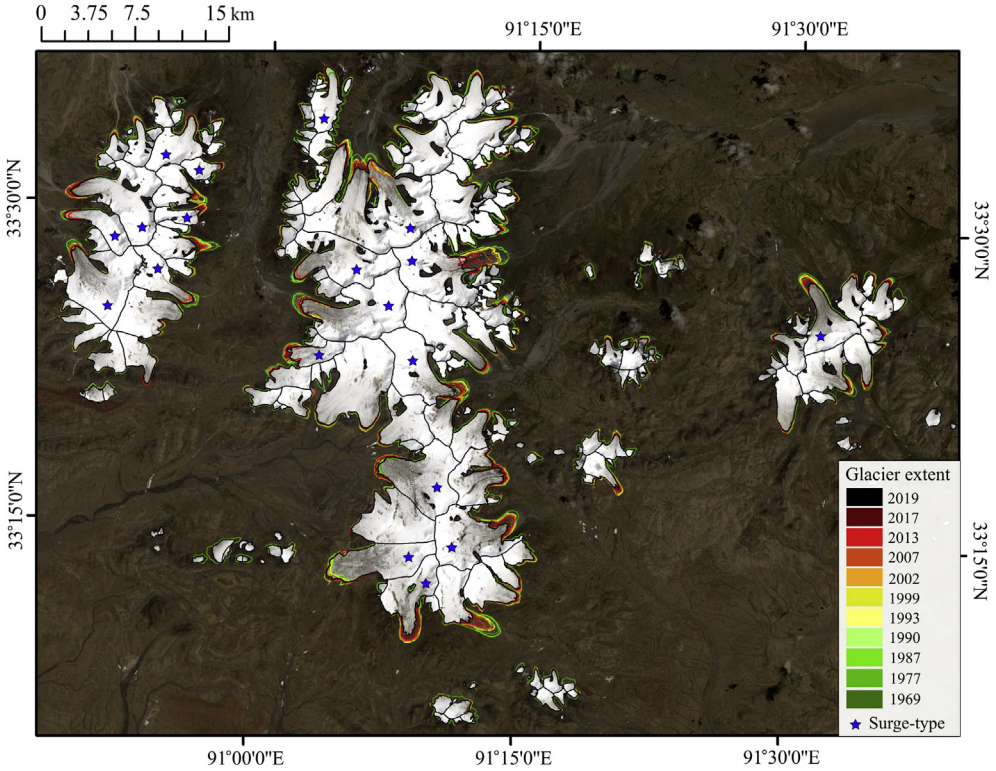

Fig. 1. The Geladandong ice caps on the Tibetan Plateau (Glacier extents have been digitised using orthoimages covering the period 1969–2019 as a reference for each epoch. Surge-type glacier identification is based on evidence of glacier area, glacier surface velocity and glacier surface elevation change indicators. Background imagery is a Landsat OLI scene from 2019).

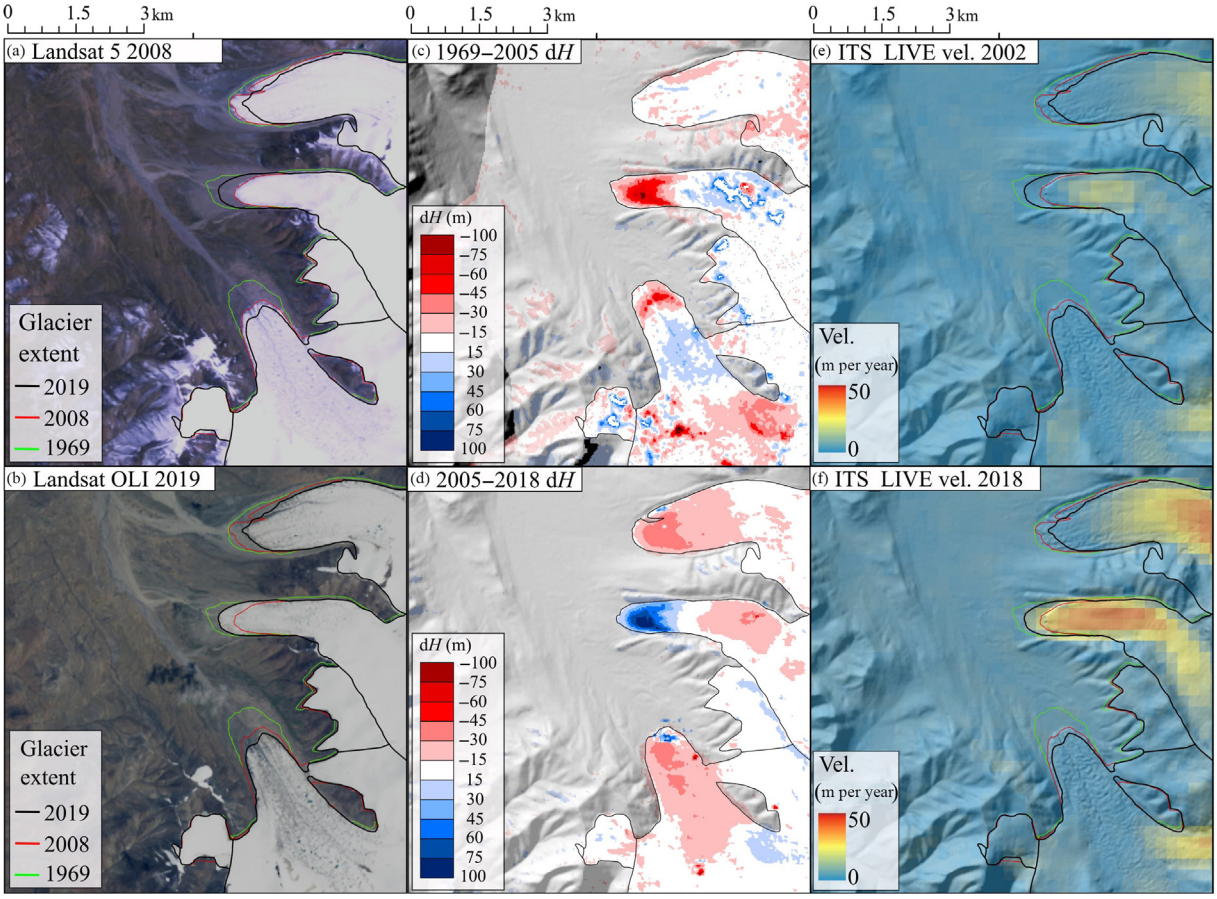

Fig. 2. Examples of glacier area change (a, b), glacier surface elevation change (c, d) and glacier surface velocity (e, f) data used to identify surge-type glaciers of the Geladandong ice cap (A hillshade of the ALOS PRISM DEM underlies semi-transparent off-glacier dH and surface velocity data in panels c–f).

Aðalgeirsdóttir et al., 2005). The impact of widespread glacier surging on glacier mass loss rates is yet to be considered in the Tibetan Plateau.

In this study we aim to examine the evolution of the area, mass budget and surface velocity of the Geladandong ice cap glaciers over a multi-decadal time period to better understand sources of variability in ice loss at the intra-regional scale on the Tibetan Plateau. To do so, we generated a geodetic time series of glacier surface elevation change measurements, a record of glacier area changes and an inventory of glacier surge events over the ice caps since the 1960s using a variety of remotely sensed datasets. We use our results to consider the impact of pervasive glacier surging on regional ice mass budgets and the threat posed by associated glacier hazards.

2. Materials and methods

The data generated in this study is based solely on remotely sensed imagery. We examine glacier area and glacier surface elevation change over the last 5 decades over the Geladandong ice caps (Fig. 1) using imagery collected by the Corona KH-4, Advanced Spaceborne Thermal Emission Reflection Radiometer (ASTER) and different Landsat sensors (Table 1).

2.1. DEM generation

We generated DEMs from Corona KH-4 imagery using the Remote Sensing Software Package Graz (RSG). Our workflow for generated Corona DEMs mirrors that thoroughly described by Goerlich et al. (2017). We processed subsets of overlapping Corona image strips, initially constraining camera orientation parameters using GCPs. A specific image distortion model developed by RSG was used to derive an initial geometric model, which was also refined using GCPs with triangulation residuals of less than 2.5 pixels. Stereo pairs were coregistered using an automated tie point measurement tool which used a Förstner operator (Goerlich et al., 2017) to detect suitable points, focussing on the forward image (Förstner and Gülch, 1987). Image matching disparity predictions and thorough image quality and back-matching filters were applied to identify and remove mismatched pixels prior to DEM generation.

We used the open source automated DEM mass production Ames Stereo Pipeline (ASP) developed by the National Aeronautics and Space Administration (NASA), and adapted by Shean et al. (2016), to generate DEMs from ASTER L1A imagery. We pre-processed raw imagery to generate an approximate Rational Polynomial Coefficient (RPC) camera model and corresponding nadir (3N) and backward looking

Table 1
Sources of data used in this study to examine glacier area, glacier surface elevation (dH/dT) and glacier mass balance changes.

Data source	Date	Purpose
Corona KH–4B	Dec 13, 1969	Glacier area, dH/dT & mass balance
ASTER	Dec 8, 2005	dH/dT & mass balance
ASTER	Feb 26, 2006	dH/dT & mass balance
ASTER	Dec 2, 2017	dH/dT & mass balance
ASTER	Jan 1, 2018	dH/dT & mass balance
Brun et al. (2017) dH/dT	2000–2015	Surge-type glacier dH/dT
SRTM-ALOS AW3D30	2000–2006/11	Surge-type glacier dH/dT
Landsat MSS	Nov 12, 1976	Glacier area
Landsat 5	Jan 22, 1987	Glacier area
Landsat 5	Oct 30, 1990	Glacier area
Landsat 5	Dec 12, 1993	Glacier area
Landsat 5	April 13, 1999	Glacier area
Landsat 7 ETM+	May 15, 2003	Glacier area
Landsat 5	April 19, 2007	Glacier area
Landsat 8 OLI	March 23, 2013	Glacier area
Landsat 8 OLI	Dec 10, 2017	Glacier area
Landsat 8 OLI	July 25, 2019	Glacier area
ITS_LIVE	1988–2017	Glacier surface velocity

(3B) images. We orthorectified each stereo pair and generated a point cloud considering standard photogrammetric principles, which was interpolated and geocoded to produce 30 m resolution DEMs. We used 4 DEMs generated from ASTER imagery to derive glacier surface elevation change estimates over the period 2005/06–2017/18 over both Geladandong ice caps (Table 1).

2.2. DEM post-processing and mass balance estimation

The geolocation of DEMs generated from imagery acquired by different sensors needs to be consistent prior to the derivation of surface elevation change estimates. We followed the approach of Nuth and Kääb (2011) to minimise stable-ground elevation differences in x, y and z directions between DEMs from different epochs using the Shuttle Radar Topographic Mission (SRTM) DEM as a reference surface. Elevation dependant biases related to tilts between DEMs were estimated and removed using first order polynomial trend surfaces relative to the SRTM DEM (Pieczonka et al., 2013). Following DEM differencing, we removed erroneous values of surface elevation change over glacier areas, which predominantly occur over ice due to low image contrast or topographic shading in areas of extreme relief, using an elevation-dependent sigmoid function (Pieczonka and Bolch, 2015). We employed the approach of Pieczonka and Bolch (2015), which allows for a variable threshold of elevation change to be applied through the elevation range of glacier, because of the prevalence of surge-type glaciers in the region. Surge-type glacier behaviour causes contrasting patterns of glacier surface elevation change when compared to usual patterns of clean-ice glacier thinning in response to climate change.

We converted glacier surface elevation change data to estimates of individual glacier mass balance. We filled data gaps caused by outlier removal or by unsuccessful interpolation during the DEM generation process using median values of elevation change from pixels within the same 100 m elevation bin following McNabb et al. (2019). Glacier extents for each point in our time series were digitised using RGI V6.0 (RGI Consortium, 2017) as a baseline inventory which was modified using the Corona KH-4, ASTER and Landsat scenes from different years (Table 1). The Corona KH-4 and ASTER imagery we used to generate DEMs were acquired at a similar time of year and we, therefore consider that they capture glacier surface conditions at comparable points in the annual cycle of accumulation and ablation. We do not apply any seasonality correction (e.g., Chen et al., 2017) as a result. Filtered, gap filled surface elevation change data were converted to ice volume change and then ice mass change estimates considering the pixel size of elevation change grids (30 m) and a conversion factor of 850 ± 60 kg m^3 (Huss, 2013).

2.3. Ancillary dataset analyses

We examined changes in glacier dynamics accompanying glacier surface elevation and glacier extent change using the ITS_LIVE dataset of glacier surface velocity (Gardner et al., 2020). The ITS_LIVE data have been generated through the automated tracking of glacier surface features present in Landsat scenes captured by the Landsat 5 (1984–1999), Landsat ETM (1999–2013) and Landsat OLI (2013 onwards) archives and using the AUTO-RIFT pipeline (Gardner et al., 2018). We extracted annual velocity profiles along manually digitised glacier centreline profiles (Fig. 3) for surge-type glaciers over the period 1988–2018.

In addition to the surface elevation change data derived through the differencing of Corona and ASTER DEMs, we used the SRTM DEM and ALOS PRISM DEMs to derive glacier surface elevation change estimates over the period 2000–2006/11 over the Geladandong ice caps. We also used the surface elevation change data generated by Brun et al. (2017) to complete the coverage over glacier areas over the period 2000–2015. We followed the same coregistration and data filtering steps described above to derive elevation change from the SRTM and ALOS PRISM DEMs, but do not use these data to estimates glacier mass balance. We used these surface elevation change data to better understand the style of surge development over the Geladandong ice caps (Figs. 5 and 6).

2.4. Identification of surge-type glaciers

We classified glaciers as surge-type based on three main diagnostic criteria (cf. Copland et al., 2011; Bhambri et al., 2017; Goerlich et al., 2020). Firstly, evidence of rapid glacier terminus advance, in direct contrast to the regional trend of glacier recession, was taken to indicate glacier surging. Second, surface velocity acceleration over part or all of a glaciers surface indicated by the ITS_LIVE glacier velocity time series was taken to indicate the initiation of the active phase of the surge cycle. Third, substantial, spatially

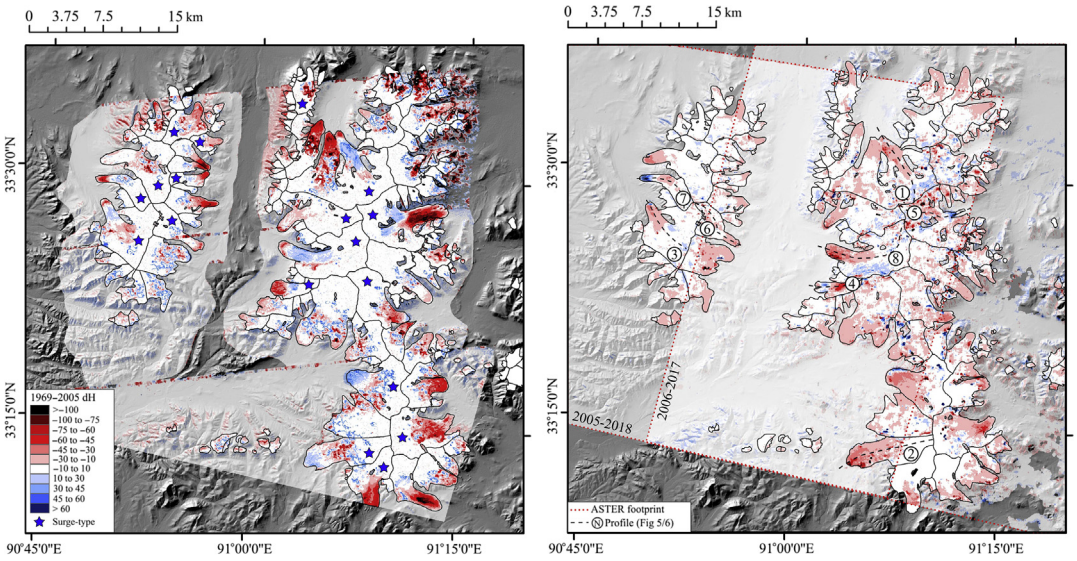

Fig. 3. Change in surface elevation between Corona and ASTER DEMs (1969–2005/2006, left) and ASTER DEMs (2005/2006–2017/2018, right) over the Geladandong ice caps. Numbers on right hand panel refer to glaciers shown in Figs. 5 and 6.

concentrated glacier surface elevation changes either in glacier reservoir (higher reaches) or receiving zones (lower reaches) (Fig. 2) were taken to indicate ice mass transfer associated with the surge-phase. Morphological evidence such as the looping of medial moraines, widespread crevassing and the development of shear margins were used to confirm surge-type glacier classification. However, where the presence of morphological features such as crevasse networks or contorted medial moraines were the only lines of evidence indicating surge behaviour we did not classify a glacier as surge-type as other factors could also cause their formation.

2.5. Uncertainty

We estimate the uncertainty associated with surface elevation, volume and glacier mass changes following the approach of Fischer et al. (2015); a simplification of the methods developed by Rolstad et al. (2009). Such an approach treats uncertainty associated with the rate of elevation change, the uncertainty associated with glacier area and uncertainty associated with volume to mass conversion independently. The uncertainty associated with the rate of elevation change is derived by:

$$\sigma_{\Delta z,g} = \sqrt{\sigma^2 \Delta h_g \bullet \frac{A_{\mathrm{cor}}}{5 \bullet A_{T1}}} \tag{1}$$

where $\sigma^2 \Delta h_g$ (m) is the standard deviation of elevation change estimates over stable terrain, A_{cor} is the length of spatial autocorrelation within elevation difference data and A_{T1} is the glacier area at the start of the time period over which elevation change is being measured. We assume $A_{T1}$to be greater than A_{cor} in all cases. We find correlation lengths varying from 123 to 509 m, depending on the time period and combination of DEMs used to derive surface elevation change estimates. The uncertainty associated with volume change is derived by multiplying $\sigma_{\Delta z,g}$ with A_{T1} which yields total, region wide uncertainty estimates of volume change ranging from ±0.29–0.78 km^3, again depending on the time period and combination of DEMs. Geodetic mass balance uncertainty $\sigma_{geod,\,g}$ (m w.e.) is estimated following Huss et al. (2009) and Fischer et al. (2015), whereby:

$$\sigma_{geod,\,g} = \sqrt{\left(\Delta z, g \bullet \sigma_{f\Delta V}\right)^2 + \left(f\Delta V \bullet \sigma_{\Delta z,g}\right)^2} \tag{2}$$

in which we employ a conversion factor $(f\Delta V)$ of 0.85 and a corresponding uncertainty $(\sigma_{f\Delta V})$ of 0.06 (Huss, 2013). Values of $\sigma_{geod,\,g}$ vary from ±0.06 to ±0.17 m w.e. per year for different time periods. We estimate the uncertainty associated with our time series of glacier area change estimates by considering that glacier outlines are accurate to within ±1 pixel (Paul et al., 2013), thus our uncertainty estimates for different epochs reflect the source imagery used to map glacier area (Fig. 7).

3. Results

3.1. Geladandong glacier surging

We identified 19 surge-type glaciers around the Geladandong ice caps (Figs. 1 and 3). Seven of these glaciers are located in the western ice cap; 11 are located in the eastern (main) ice cap and one is located amongst a smaller group of glaciers approximately 40 km east of Geladandong east ice cap. Of the 19 surge events we identified, we captured substantial elevation change over 11 glaciers. Clear surface velocity changes are evident over 12 of these glaciers and surge-type classification is based solely on terminus position changes in four cases. In these four cases, terminus advance occurred between the 1969 Corona KH-4 acquisition and the first available Landsat MSS scene acquired in 1977.

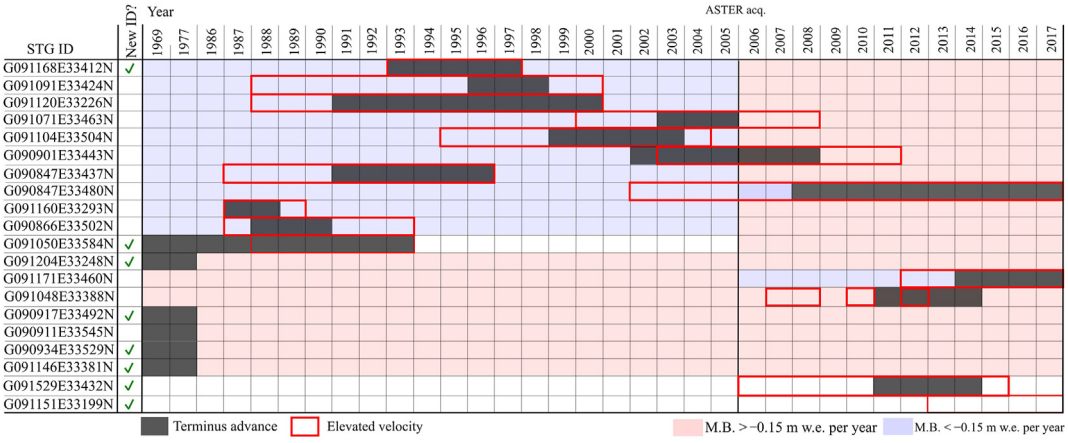

Fig. 4. Chronology of the surge-type glaciers of the Geledandong ice cap between 1969 and 2017 (A mass balance threshold of −0.15 m w.e. per year was used to distinguish between glaciers losing ice at a suppressed rate (shaded blue) during late quiescence and their active phase and glaciers losing ice at an enhanced rate (shaded red) in early/mid quiescence following surge events, considering the uncertainty associated with glacier mass balance estimates).

The intensity and magnitude of surge-phase ice mass transfer varied from glacier to glacier. Maximum glacier thickening in association with surging varied from 30 to 100 m (Fig. 3). Terminus position change varied from 0 m, where a glaciers surge terminated amongst stagnant, thinning ice and did not cause an advance, to 675 m. Maximum measured surge-phase surface velocities ranged from 35 m per year to up to 160 m per year, although typically ranged from 45 to 75 m per year.

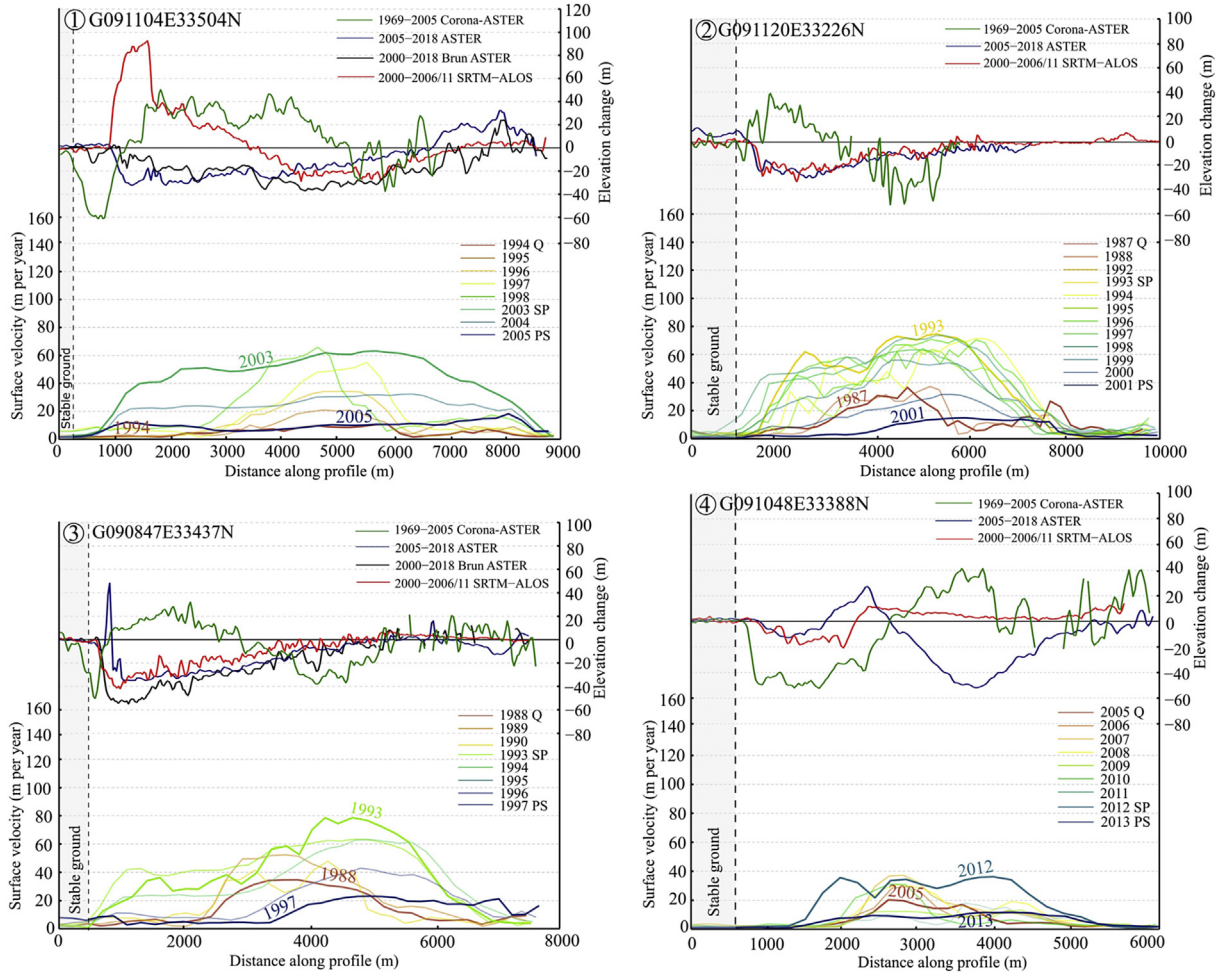

Fig. 5. Examples of elevation and velocity changes during surge events of four glaciers of the Geladandong ice cap where uniform velocity increases spread both up and down-glacier during the surge phase (Glacier surface velocity data have been extracted from the ITS_LIVE dataset of Gardner et al. (2020). The down-glacier direction is from right to left in all cases).

The mean length of the active phase of the 12 glaciers we could fully resolve was 9 years, ranging from 3 to 15 years (Fig. 4).

Analyses of the ITS_LIVE glacier surface velocity data shows two distinct styles of velocity field evolution during the 13 surge events covered by this dataset. In eight cases, increased surface velocities associated with the surge phase effected almost the entire length of each glacier, whereby an initial acceleration of ice flow occurred in the middle reaches of each glacier and was followed by a spatially uniform increase of glacier surface velocity in both glacier reservoir and receiving zones (Fig. 5). Large regions of these glaciers experienced flow rates close to each glaciers maximum surge-phase velocity (Fig. 5). In contrast, five of the surge-type glaciers we identified displayed spatially restricted elevated surface velocities which migrated down-glacier as each surge developed, four of which are shown in Fig. 6. Peak surge-phase velocities effected smaller portions of these five glaciers and were generally measured close to each glaciers advancing terminus.

The pattern of glacier surface elevation change amongst the 12 surge events covered by our dH data could not be subdivided in the same way as the surface velocity data over the same glaciers. In all but two of these twelve cases a distinct zone of spatially concentrated thickening developed in the receiving zone of each glacier and reached their termini before the end of the surge-phase. In the two cases where the surge front did not reach the glacier termini, stagnant, downwasting ice was present further down-glacier (Fig. 5).

3.2. Glacier area changes

Glacier area reduced by 65 km^2 between 1969 (719 ± 5 km^2) and 2019 (655 ± 19 km^2) over the Geladandong ice caps, a 9% reduction in glacier area over the full study period. Glacier surging did not compensate for region wide glacier area losses around the Geladandong ice caps. Surge-type glaciers around the Geladandong ice caps reduced in area by about 15 km^2 between 1969 (338 ± 2 km^2) and 2019 (313 ± 6 km^2), although the rate of glacier area loss from non-surge-type glaciers (0.8 ± 0.08 km^2 per year) was markedly above that of surge-type glaciers (0.3 ± 0.08 km^2 per year) here (Fig. 7).

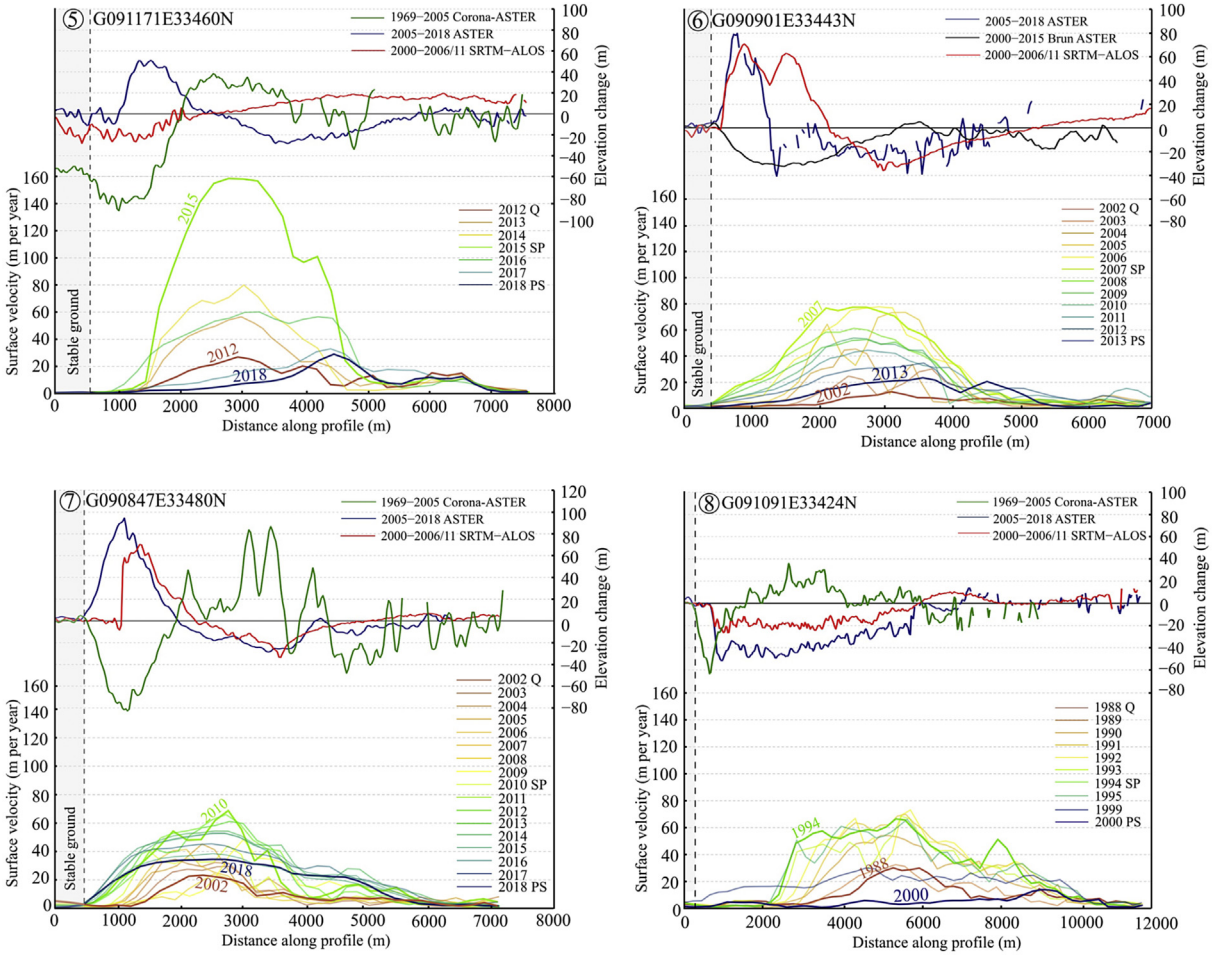

Fig. 6. Examples of surge events from four glaciers of the Geladandong ice cap where spatially concentrated surface velocity increases migrated down-glacier during the surge phase (Glacier surface velocity data have been extracted from the ITS_LIVE dataset of Gardner et al. (2020). The down-glacier direction is from right to left in all cases).

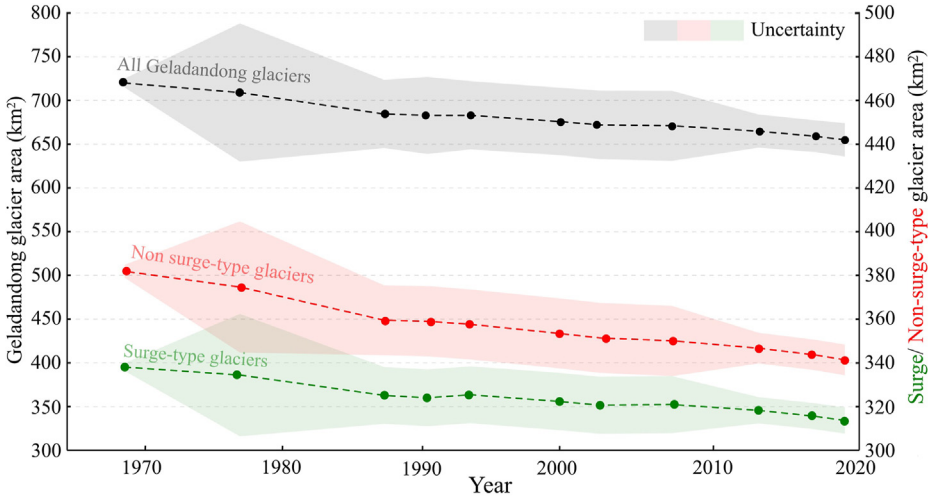

Fig. 7. Glacier area change over the Geladandong ice caps between 1969 and 2019.

Table 2
Geodetic mass balance estimates for the glaciers of the Geladandong ice caps over the different study periods.

Region	Period	Coverage (km^2)	Mass balance (m w.e. per year)
Geladandong	1969–2005	442	−0.18 ± 0.08
Geladandong	1969–2017/2018	412	−0.24 ± 0.07/0.09
Geladandong	2005/2006–2017/2018	476	−0.48 ± 0.06/0.17

Table 3
Geodetic mass balance estimates of surge-type glaciers depending on the stage of their surge cycle, along with non-surge-type glaciers around the Geladandong ice cap.

Glacier type	Period	Number of glaciers	Mass balance (m w.e. per year)
Pre-surge	1969–2005	10	−0.06 ± 0.08
Mid-quiescence	1969–2005	7	−0.16 ± 0.08
All surge-type	1969–2005	17	−0.12 ± 0.08
Non-surge-type	1969–2005	22	−0.23 ± 0.08
Pre-surge	2005/2006–2017/2018	2	−0.09 ± 0.12
Mid-quiescence	2005/2006–2017/2018	11	−0.48 ± 0.12
All surge-type	2005/2006–2017/2018	13	−0.42 ± 0.12
Non-surge-type	2005/2006–2017/2018	44	−0.50 ± 0.12

3.3. Glacier surface elevation change and mass balance

Glaciers of the Geladandong ice cap thinned at a mean rate of −0.27 ± 0.10 m per year and lost mass at a mean rate of −0.24 ± 0.08 m w.e. per year over the full (1969–2018) study period. The greatest thinning (up to 110 m between 1969 and 2018) in this area occurred over glacier tongues situated below ~5500 m a.s.l., many of which have now retreated to higher altitudes (Fig. 1). The rate of thinning and mass loss around the Geladandong ice caps increased across our two study periods. Between 1969 and 2005/06, the mean rate of thinning over all glacier surfaces was −0.22 ± 0.09 m per year and the mean mass balance was −0.18 ± 0.08 m w.e. per year which increased to −0.66 ± 0.08 m per year and −0.48 ± 0.07 m w.e. per year between 2005/2006 and 2017/2018 (Table 2).

Over the full study period (1969–2017/2018), the mass balance of surge-type (−0.19 ± 0.08 m w.e. per year) and non-surge-type glaciers (−0.26 ± 0.08 m w.e. per year) were not substantially different from one another. Over the period 1969–2005 surge-type glaciers of the Geladandong ice cap lost ice at a lower rate (−0.12 ± 0.08 m w.e. per year) when compared to non-surge-type glaciers (−0.23 ± 0.08 m w.e. per year). Between 2005/2006 and 2017/2018, the mass loss rate of surge-type glaciers (−0.42 ± 0.12 m w.e. per year) was again comparable to the regional (−0.48 ± 0.12 m w.e. per year) rate of mass loss as well as non-surge-type glaciers (−0.50 ± 0.12 m w.e. per year). However, discrete variability in the mass loss rate of surge-type glaciers is evident when their mass balance is compared on an individual basis, across both time periods. Low mass loss rates or even balanced mass budgets were measured for 10 surge-type glaciers over the period 1969–2005 (Table 3). These 10 glaciers surged towards the end of the initial (1969–2005) study period of DEM differencing (Fig. 4). We consider these glaciers as being in a pre-surge state over the majority of the 1969–2005 study period. The other seven surge-type glaciers for which we could generate mass balance estimates over this initial time period displayed much greater ice mass loss rates (Table 3). These seven glaciers surged either between 1969 and 1977 or after the intermediate timestep (2005/2006) of our time series (Fig. 4). We consider these seven glaciers to be in a mid-quiescent state over the initial study period.

The mass loss rate of the ten ‘pre-surge’ glaciers identified using the 1969–2005 DEM difference data changed markedly

in our second time period following their surge events. Between 2005/2006 and 2017/2018 these same ten glaciers lost ice at a mean rate of −0.35 ± 0.12 m w.e. per year, compared to −0.06 ± 0.08 m w.e. per year in the preceding time period. The seven 'mid-quiescent' glaciers also lost ice at an increased rate (mean −0.43 ± 0.12 m w.e. per year), compared to the previous time period, although accelerated mass loss was not ubiquitous between these glaciers. Of these seven glaciers, the mass loss rate of four increased markedly over the two study periods, and the mass loss rate of three decreased over the two time periods (Figs. 4 and 8).

Separating the mass balance estimates of surge-type glaciers for the contemporary time period using the same criteria used in the 1969–2005 period again indicates differing mass loss rates depending on the phase of a glaciers surge-cycle. Two glaciers which began to surge in the middle of this later time period, and can therefore be described as in a pre-surge state at the beginning of the contemporary study period, displayed low mass loss rates (mean −0.09 ± 0.08 m w.e. per year) in comparison to the regional mass balance (Table 2). Surge-type glaciers in their 'mid quiescent' phase lost ice at a much greater rate over this second time period (n = 11, mean −0.48 ± 0.12 m w.e. per year).

4. Discussion

4.1. Ice mass budget of the Tanggula mountains

Our geodetic mass balance estimates indicate a substantial increase in the mass loss rate from glaciers of the Geladandong ice caps since the 1960s. Our mass balance estimates derived from Corona KH-4 and ASTER DEMs (−0.18 ± 0.08 m w.e. per year from 1969 to 2005/2006) agree with those derived by Chen et al. (2017) and Zhou et al. (2018) over a similar period (−0.21 ± 0.18 m w.e. per year from 1969 to 1999 and −0.22 ± 0.12 from 1976 to 2000, respectively), despite differences in the data used to generate DEMs and the extent of coverage between our studies. Our estimates of mass loss over the period 2005–2018 differ somewhat to those of Chen et al. (2017), although not in a statistically significant way owing to their broad uncertainty range. Over both Geladandong ice caps, we derived a mean mass loss rate of −0.48 ± 0.06 m w.e. per year from 2005 to 2018, in comparison to the estimate of −0.33 ± 0.38 m w.e. per year given by Chen et al. (2017). Our geodetic mass balance estimates suggest that ice mass loss rates at the western end of the Tanggula mountains have more than doubled since the late 1960s.

The differences in the contemporary mass balance estimates we have derived when compared to Chen et al. (2017) may be attributable to several methodological factors including contrasting data coverage extents, C-band radar wave ice surface penetration biases and the application of suitable dH data gap filling methods. If left uncorrected, C-band radar wave penetration may cause the underestimation of regional mass balance by up to 20% (Vijay and Braun, 2016). The addition of 20% to the mass loss budget of Chen et al. (2017) does not reconcile the difference between our estimates of mass loss over the Geladandong ice caps since the millennium. This may suggest an underestimate of C-band radar wave penetration in the study of Chen et al. (2017), although Zhou et al. (2018) derived very similar estimates of C-band radar wave penetration over other Tibetan Plateau ice caps. Using an alternative method to derive C-band penetration estimates, Kääb et al. (2015) suggest much greater biases (7–10 m) over the southeastern Tibetan Plateau which would cause a greater discrepancy if uncorrected for, but their study period (2003–2009) may not be representative of longer periods. Similarly, the choice of appropriate methods to filter erroneous dH data and to fill resulting data gaps, which are common over saturated areas of optical stereo imagery of moderate spatial and radiometric resolution, are important to avoid the introduction of substantial bias into elevation change data (McNabb et al., 2019). McNabb et al. (2019) showed how 'local' gap filling methods, which involve the calculation of average elevation change estimates within the elevation range of individual glaciers, introduce very little bias (<1% difference) into estimates of elevation change, and therefore glacier mass balance, when compared to non-voided elevation change data. The application of such methods are particularly important in regions containing surge-type glaciers where glacier to glacier variability in elevation change gradients can be extreme. Information on the treatment of outliers or data gaps is not forthcoming in Chen et al. (2017) and the impact of such factors on their results is therefore unknown. The most likely explanation for the differences in mass loss estimates over the Geladandong ice caps is contrasting data coverage. We were able to derive glacier mass balance estimates for 62%–72% (depending on the coverage of different ASTER scenes) of total glacier area, in comparison to ~23% of the total glacier area covered by Chen et al. (2017). We note strong ice loss from the larger glaciers of the eastern ice cap here, particularly those which surged towards the end of our first study period (1969–2005, Fig. 5) and have seen widespread thinning since (Fig. 3). We therefore suggest that our higher contemporary mass loss estimates are more

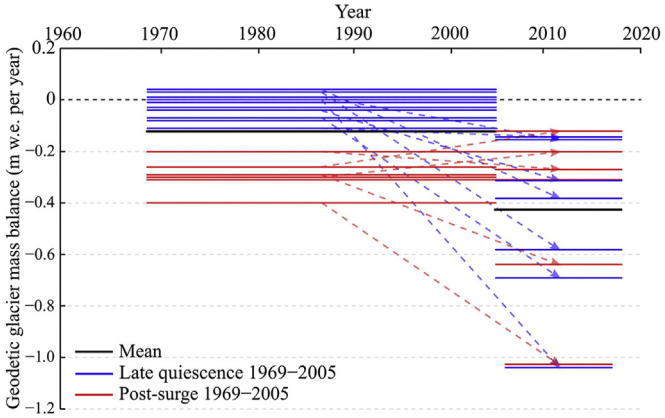

Fig. 8. The evolution of the mass balance of surge-type glaciers of the Geladandong ice caps depending on the stage of their surge cycle covered by geodetic measurements over different time periods.

representative of current glacier behaviour over the Geladandong ice caps.

4.2. The influence of glacier surging on mass balance

When considered collectively, the mass loss rate of surge-type glaciers of the Geladandong ice caps are comparable to non-surge-type glaciers in the region and have been since the late 1960s (Table 3). The similarity of the mass budget of surge-type glaciers to the regional mean mass budget of non-surge-type glaciers has been noted elsewhere in HMA (Gardelle et al., 2013; Bolch et al., 2017; Berthier and Brun, 2019; Lv et al., 2019) and in other surge-type glacier clusters (Kochtitzky et al., 2020). Surge-type behaviour still occurs during periods of negative mass balance as long as glaciers can still accumulate ice mass in their reservoir zones, although the extent of surge events may decline as mass loss persists from the host glacier (Frappé and Clarke, 2007; Kochtitzky et al., 2020) and long-term climatic change may ultimately cause the cessation of surge behaviour from a glacier (Hoinkes, 1969; Christoffersen et al., 2005; Kochtitzky et al., 2020). The initiation of six surges since 2000 around the Geladandong ice caps would suggest that, despite recent warming in the area (Chen et al., 2017), the local climate remains suitable for surge-type glacier behaviour (Sevestre and Benn, 2015).

The further subdivision of our mass balance estimates suggests that glaciers at a certain stage of their surge cycle display suppressed mass loss rates compared to the local, non-surge-type glacier population. Considering the chronology of surge events shown in Fig. 4, we identified ten surge-type glaciers where mass loss rates were lower (mean -0.03 ± 0.08 m w.e. per year, ranging from -0.11 ± 0.08 to 0.04 ± 0.08 m w.e. per year) than the rest of the surge-type glacier population (mean -0.30 ± 0.08 m w.e. per year, ranging from -0.20 ± 0.08 to -0.40 ± 0.08 m w.e. per year) from 1969 to 2005. The mass balance of these ten surge-type glaciers was also lower than that of non-surge-type glaciers (mean -0.23 ± 0.08 m w.e. per year) over the period 1969–2005. These ten glaciers experienced their active surge phase either shortly before (<15 years) or during the acquisition date of the 2005/2006 ASTER scenes covering the Geladandong ice caps. The mean mass balance of the other seven surge-type glaciers (-0.30 ± 0.08 m w.e. per year) for which we could generate mass balance estimates was more negative and even slightly above the regional mean (-0.18 ± 0.08 m w.e. per year) over the 1969–2005 period. The active phase of these seven other surge-type glaciers occurred towards the start of our first observation period, close to the acquisition date of the Corona KH-4 dataset (Fig. 4).

Similar differences were replicated in our contemporary mass balance estimates. The two glaciers whose surges began shortly after the 2005/2006 acquisition date of the ASTER scenes displayed low mass loss rates (-0.09 ± 0.12 m w.e. per year) when compared to surge-type glaciers not displaying active surge behaviour at during this time period. The remaining 11 surge-type glaciers for which we could derive mass balance estimates displayed a mass loss rate (-0.48 ± 0.12 m w.e. per year) identical to the regional mean (-0.48 ± 0.12 m w.e. per year) over this later time period. The 10 surge-type glaciers which displayed suppressed mass loss rates (-0.03 ± 0.08 m w.e. per year) in the earlier time (1969–2005) period lost ice at a much greater rate (-0.35 ± 0.12 m w.e. per year) over our more contemporary (2005/2006–2017/2018) time period (Fig. 8).

We suggest that the differences in surge-type glacier mass balance described above depend on which portion of the quiescent phase and/or early surge phase is captured by the observation period of DEM difference data. Should the observation period of dH data capture the period immediately following surge cessation, when a large volume of ice has been transported to warmer, lower elevations, the thinning captured will be substantial (Sund et al., 2009; Yde and Knudsen, 2007; Aðalgeirsdóttir et al., 2005). Over a decadal period, the timespan covered by many contemporary geodetic glacier mass loss studies, mass build up in the glaciers reservoir zone will not offset this ablation and the mass balance of the glacier will be negative. The substantial mass loss we measured between 2005/2006 and 2017/2018 from glaciers which surged shortly (<15 years) before 2005 is evidence of this process. Levels of ablation in the years immediately following the surge phase are likely to be particularly enhanced in the case of Geladandong glaciers because of their lack of insulating debris over their lower reaches.

In contrast, should dH data capture the later stages of quiescence, mass loss and therefore mass balance from a surge-type glacier may be suppressed. In this scenario, the recorded elevation changes will reflect the final stages of pre-surge mass build up in the glaciers reservoir zone, but the low lying terminus formed by the previous surge will have thinned and retreated to a higher altitude earlier in quiescence, as long as substantial debris cover has not inhibited its retreat. The rate of thinning around the new terminus position will be lower at this higher altitude and the mass balance of each glacier less negative. The comparatively low mass loss rate from 10 glaciers which surged close to the 2005 ASTER acquisition used to generate dH data over the period 1969–2005 provides evidence of this scenario. When averaged collectively, the enhanced mass loss from glaciers in a post surge-phase and diminished mass loss from glaciers approaching a pre-surge state seem to reflect the mass loss rate from non-surge-type glaciers in the same region.

4.3. Characterising Tibetan Plateau surges

When compared to other surge-type glacier clusters found elsewhere in High Mountain Asia (e.g. Karakoram (Bhambri et al., 2017), Tien Shan (Mukherjee et al., 2017), West Kunlun Shan (Yasuda and Furuya, 2015), Pamir (Goerlich et al., 2020)), relatively little is known about the prevalence and characteristics of surge-type glaciers on the Tibetan Plateau (Sevestre and Benn, 2015). A growing body of literature suggests that surge-type glaciers are not uncommon in the ice caps of the north and North Eastern Tibetan Plateau. Surge-type behaviour has recently been identified within glaciers

of the Xinqingfeng and Malan ice caps (Zhang et al., 2020) and the Ulugh Muztag (Jiang et al., 2012) in the Eastern Kunlun Shan, the Duxeshan, Burog Kangri and Zangser Kangri (Zhang et al., 2020) of the Tibetan Interior Mountains, the Amney Machen (Paul, 2019) of the Eastern Tibetan Mountains and the Qilian mountains (Xu et al., 2013) of the Qilian Shan. Fewer examples of surge-type glacier behaviour have been documented in the southern and south eastern Tibetan Plateau (Gandise Mountains, western Nyainqentanghla) (e.g. Wu et al., 2018) where the climate is notably different, although still within the climatic envelope required for surge-behaviour described by Sevestre and Benn (2015). The concentration of surge-type glaciers around the Geladandong ice caps appears to be greater than anywhere else on the Tibetan Plateau.

Around the Geladandong ice caps, Chen et al. (2017) and Xu et al. (2018) identified eleven of the same surge-type glaciers we have identified, but eight of the surge events we have identified have not been documented before (Fig. 4). Xu et al. (2018) identified two glaciers as surge-type which we do not as the slight changes in terminus position they experienced were not greater than the pixel size of the imagery used to identify their advance (Landsat MSS). Additional evidence of surge behaviour (surface elevation or surface velocity changes) was not available for these two glaciers. The magnitude of thinning over several of the Geladandong ice caps main outlet glaciers which are not currently classified as surge-type, particularly at the southern edge of the eastern ice cap, seems more comparable to the post-surge phase thinning we have described for several surge-type glaciers rather than the thinning observed over the termini of non-surge-type glaciers. It is reasonable to expect that several of these large outlet glaciers are also surge-type. The active phase of three of the 19 surge-type glaciers we identified was ongoing at the point of our latest observation date (2017).

The mean length of the active phase, which we take as the duration of elevated surface velocities and/or terminus advance, of the 19 surge events we identified is about 9 years. This is longer than surge-type glaciers found in maritime climates such as Alaska and Svalbard (Sevestre and Benn, 2015), but comparable to the characteristics of surge events found elsewhere in High Mountain Asia (e.g. Bhambri et al., 2017; Lv et al., 2019; Mukherjee et al., 2017). Peak surge-phase velocities indicated by the ITS_LIVE dataset (60–80 m per year in most cases, up to a maximum of 160 m per year) are akin to surge-type glaciers in mountain ranges such as the Tien Shan (Mukerhjee et al., 2017) and eastern Pamir (Lv et al., 2019), but lower than those of the larger glaciers found in the Karokoram (e.g. Quincey et al., 2011, 2015; Heid and Kääb, 2012; Paul, 2015; Guo et al., 2020). Similar comparisons can be drawn regarding the magnitude of glacier surface elevation change experienced by Geladandong surge-type glaciers. Glacier terminus thickening generally did not exceed 100 m in our data (Figs. 5 and 6) and was always focussed around glacier termini. Mukherjee et al. (2017) measured similar magnitudes of surge-phase thickening over glaciers in the Tien Shan, as did Zhou et al. (2018) in the Western Kunlun Shan. Surge-type glaciers in the Karakoram can experience almost twice the amount of surface elevation increase over broad areas of their receiving zones (e.g. Guo et al., 2020). Generally, it seems that the increased ice flux caused by a glacier surge is of comparable magnitude across the Tibetan Plateau and in peripheral mountain ranges of HMA such as the Tien Shan.

Two styles of surge development can be identified from the compilation of glacier area, glacier surface velocity and glacier surface elevation change data. In eight of the 19 cases of surge behaviour, increased surface velocities and surface elevation increases were restricted to the receiving zone of surging glaciers (e.g. Fig. 6). In these cases, increased flow initiated several kilometres from glacier termini and generally spread down-glacier as a clear surge front, with limited impact on the surface elevation or surface velocity of ice in the reservoir zone of each glacier as the surge peaked (Fig. 6). In five cases, the surge phase impacted the flow regime of a much greater portion of the full length of each glacier. These five glaciers experienced consistent surface flow increases in their reservoir and receiving zones as each surge developed (Fig. 5). One possible distinguishing factor between these two groups of glaciers is the topography of their surroundings. The eight glaciers which developed a clear surge front are all valley-type whose termini positions, both pre and post-surge, were limited to within the confines of their host valleys. Lateral drag imparted by valley sides (e.g. Adhikari and Marshall, 2012) therefore exerts some control on the flow of the full length of these glaciers and possibly their style of surge development. The five glaciers whose surges effected their full length have unconfined termini and are more piedmont type. Thøgersen et al. (2019) showed how slow surge propagation, perhaps a result of lateral drag in the five cases described above, leads to more prominent elevation changes in surge-events. The mean maximum thickening of the five valley surge-type glaciers was 70 m whereas the mean maximum thickening of the eight piedmont style, relatively unconfined surge-type glaciers was 42 m, thus we suspect that topography induced drag has played a role in surge propagation rate and therefore surge style in the Geladandong ice cap surges.

4.4. Implications of widespread glacier surging

The widespread occurrence of glacier surging on the Tibetan Plateau brings into focus the hazards associated with unstable glacier flow and their impact on regional glacier mass loss assessments (e.g. Jiskoot, 2011). Hazards associated with glacier surging include damage to infrastructure proximal to advancing glacier termini and the formation of ice-dammed glacial lakes which may be prone to rapid drainage (e.g. Haemmig et al., 2014). Whilst the magnitude of glacier surge events and glacier collapses are somewhat different (e.g. Kääb et al., 2018), the hazards associated with both are destructive and have the ability to heavily modify the proglacial landscape, making the thorough understanding of their prevalence particularly pertinent.

Recent examples of large-scale ice avalanches and glacier collapses at various sites across the Tibetan Plateau (e.g. Kääb et al., 2018; Paul, 2019; Zhang et al., 2018) have occurred where surge-type glaciers are also located, suggesting the two could be inextricably linked. Kääb et al. (2018) carried out a thorough investigation of the factors likely to have contributed to, or in combination caused, the twin collapses of the Aru glaciers. Kääb et al. (2018) and Gilbert et al. (2018) identified preconditioning factors such as glacier morphology (geometry and slope), bedrock lithology and thermal regime characteristics common to each of the Aru glaciers that appear to have been necessary to facilitate each catastrophic event. The key factors in the case of the Aru glaciers appears to be the recent steepening of each glaciers mass balance gradient and associated increases in driving stress. These were induced by terminus retreat and an increase in accumulation, which has also sustained an approximately balanced glacier mass budget in the western Kunlun Mountain region (Shean et al., 2020), and the input of substantial amounts of meltwater into each glacier system prior to each glacier collapse (Gilbert et al., 2018). Whilst many of the clean ice glaciers draining Tibetan Plateaus ice caps may share morphological characteristics (Sevestre and Benn, 2015), the mass budget of most is currently negative (Shean et al., 2020). The recent trend in accumulation over the Geladandong ice caps (Jenkins et al., 2016) is also negative, thus we do not expect the mass balance gradient of the glaciers we have studied to have steepened substantially in recent years. External triggers, such as rockfall loading (Paul, 2019) may be more likely to induce glacier mass movements in areas of the Tibetan Plateau where glacier mass balance is negative.

The contrast in mass balance displayed by surge-type glaciers of the Geladandong ice caps at different stages of their surge cycle suggests a careful approach should be taken when interpreting mass loss rates from glaciated regions known to contain surge-type glaciers. Whilst the differences between the mass balance of pre-surge phase and mid-quiescent surge-type glaciers seem to counter one another at the regional scale when data coverage is high, the selection of either group as a representative sample of the regional mass budget may suggest exacerbated or suppressed glacier mass loss from a region where complete data coverage cannot be achieved. The comparison of our mass balance estimates against those generated for only the western Geladandong ice cap by Chen et al. (2017) shows the importance of data coverage in regions with numerous surge-type glaciers. More detailed assessments of how the mass balance of surge-type glaciers varies in settings with extensive debris cover and where several tributary surge-type glaciers coalesce should also be undertaken to understand the applicability of our findings to areas such as the Karakoram. Extensive, thick debris cover may dampen post-surge receiving zone glacier thinning and a less negative mass balance will result. Similarly, the termination of a surge against another glacier would limit how far surging glaciers can advance down-valley to a lower elevation, again dampening post-surge melt rates.

5. Conclusions

We have examined the behaviour of glaciers draining the Geladandong ice caps since the late 1960s. Our measurements of glacier area, glacier surface elevation and glacier surface velocity change show widespread glacier retreat (9% area reduction) and ice mass loss over the study period. Our geodetic mass balance estimates show that glacier mass loss rates have likely more than doubled from the region over the periods 1969–2005/2006 (-0.18 ± 0.08 m w.e. per year) and 2005/2006–2017/2018 (-0.48 ± 0.12 m w.e. per year). Our observations also capture the surge-type behaviour of 19 glaciers emanating from both ice caps, eight of which haven't been documented in previous studies. We are able to distinguish two distinct groups within our inventory of surge-type glaciers based on their mass balance and the phase of their surge-cycle covered by geodetic datasets. The mass balance of post-surge phase surge-type glaciers was variable but in many cases substantially more negative than the regional average due to enhanced ablation over large regions of glacier tongues sitting at lower elevations post-surge. The mass balance of late-quiescent phase or active phase surge-type glaciers was slightly negative or close to balanced as geodetic data capture mass build up in glacier reservoir zones and ablation that is not elevated above terminal thinning of non-surge-type glaciers. Whilst the contrasting mass budget of these two groups of glaciers compensate for one another when included in a regional mass budget estimate, the variability between individual glaciers emphasises the need for care when using a limited number of glaciers to characterise regional mass budgets. The widespread occurrence of surge-type behaviour around the Geladandong ice caps reflects recent observations of surge-type behaviour around many other Tibetan Plateau ice caps. The dynamic behaviour of these glaciers is accompanied by a number of glacier hazards which may now be more prevalent than previously thought across the region. Further work should focus on the prevalence of glacier surging in space and time across the Tibetan Plateau and should examine the level of preconditioning towards more substantial glacier mass movements in the region.

Declaration of competing interest

The authors declare no conflict of interest.

Acknowledgments

We are grateful to Yao Tandong (Institute of Tibetan Plateau Research, Chinese Academy of Sciences) for his continuous support and Gregoire Guillet (University of St Andrews) for his comments of a draft version of this manuscript. This study was supported by the Strategic Priority Research Program of Chinese Academy of Sciences (XDA20100300).

References

Aðalgeirsdóttir, G., Björnsson, H., Pálsson, F., et al., 2005. Analyses of a surging outlet glacier of Vatnajökull ice cap, Iceland. Ann. Glaciol. 42, 23–28.

Adhikari, S., Marshall, S.J., 2012. Parameterization of lateral drag in flowline models of glacier dynamics. J. Glaciol. 58 (212), 1119−1132. https://doi.org/10.3189/2012JoG12J018.

Allen, S.K., Zhang, G., Wang, W., Yao, T., Bolch, T., 2019. Potentially dangerous glacial lakes across the Tibetan Plateau revealed using a large-scale automated assessment approach. Sci. Bull. 64, 435−445. https://doi.org/10.1016/j.scib.2019.03.011.

Berthier, E., Brun, F., 2019. Karakoram geodetic glacier mass balances between 2008 and 2016: persistence of the anomaly and influence of a large rock avalanche on siachen glacier. J. Glaciol. 65, 494−507. https://doi: 10.1017/jog.2019.32.

Bhambri, R., Hewitt, K., Kawishwar, P., et al., 2017. Surge-type and surge-modified glaciers in the Karakoram. Sci. Rep. 7 (1), 15391. https://doi: 10.1038/s41598-017-15473-8.

Bolch, T., Pieczonka, T., Mukherjee, K., et al., 2017. Brief communication: glaciers in the Hunza catchment (Karakoram) have been nearly in balance since the 1970s. Cryosphere 11, 531−539. https://doi.org/10.5194/tc-11-531-2017.

Bolch, T., Shea, J.M., Liu, S., et al., 2019. Status and change of the cryosphere in the extended hindu Kush Himalaya region. In: Wester, P., Mishra, A., Mukherji, A., et al. (Eds.), The Hindu Kush Himalaya Assessment: Mountains, Climate Change, Sustainability and People. Springer International Publishing, Cham, pp. 209−255. https://doi.org/10.1007/978-3-319-92288-1_7.

Brun, F., Berthier, E., Wagnon, P., et al., 2017. A spatially resolved estimate of High Mountain Asia glacier mass balances from 2000 to 2016. Nat. Geosci. 10, 668−673. https://doi.org/10.1038/ngeo2999.

Brun, F., Wagnon, P., Berthier, E., et al., 2019. Heterogeneous influence of glacier morphology on the mass balance variability in High Mountain Asia. J. Geophys. Res. Surf. 124, 1−15. https://doi.org/10.1029/2018JF004838.

Chen, A., Wang, N., Li, Z., et al., 2017. Region-wide glacier mass budgets for the Tanggula Mountains between ~1969 and ~2015 derived from remote sensing data. Arctic Antarct. Alpine Res. 49, 551−568. https://doi.org/10.1657/AAAR0016-065.

Christoffersen, P., Piotrowski, J.A., Larsen, K., 2005. Basal processes beneath an Arctic glacier and their geomorphic imprint after a surge, Elisebreen, Svalbard. Quat. Res. 64 (2), 125−137. https://doi:10.1016/j.yqres.2005.05.009.

Copland, L., Sylvestre, T., Bishop, M.P., et al., 2011. Expanded and recently increased glacier surging in the Karakoram. Arctic Antarct. Alpine Res. 43 (4), 503−516. https://doi:10.1657/1938-4246-43.4.503.

Fischer, M., Huss, M., Hoelzle, M., 2015. Surface elevation and mass changes of all Swiss glaciers 1980−2010. Cryosphere 9, 525−540. https://doi.org/10.5194/tc-9-525-2015.

Förstner, W., Gülch, E., 1987. A fast operator for detection and precise location of distinct points, corners and centres of circular features. Proceedings of the ISPRS Inter-commission Conference on Fast Processing of Photogrammetric Data, Interlaken.

Frappé, T.-P., Clarke, G., 2007. Slow surge of Trapridge glacier, Yukon territory, Canada. J. Geophys. Res. Earth 112, F03S32. https://doi:10.1029/2006JF000607.

Gardelle, J., Berthier, E., Arnaud, Y., et al., 2013. Region-wide glacier mass balances over the Pamir–Karakoram–Himalaya during 1999−2011. Cryosphere 7, 1263−1286. https://doi.org/10.5194/tc-7-1263-2013.

Gardner, A.S., Moholdt, G., Scambos, T., et al., 2018. Increased West Antarctic and unchanged East Antarctic ice discharge over the last 7 years. Cryosphere 12 (2), 521−547. https://doi:10.5194/tc-12-521-2018.

Gardner, A.S., Fahnestock, M.A., Scambos, T., et al., 2020. ITS_LIVE regional glacier and ice sheet surface velocities. Data archived at National Snow and Ice Data Center. https://doi:10.5067/6II6VW8LLWJ7.

Gilbert, A., Leinss, S., Kargel, J., et al., 2018. Mechanisms leading to the 2016 giant twin glacier collapses, Aru Range, Tibet. Cryosphere 12 (9), 2883−2900. https://doi.org/10.5194/tc-12-2883-2018.

Goerlich, F., Bolch, T., Paul, F., 2020. More dynamic than expected: an updated survey of surging glaciers in the Pamir. Earth Syst. Sci. Data 12, 3161−3176. https://doi.org/10.5194/essd-12-3161-2020.

Goerlich, F., Bolch, T., Mukherjee, K., et al., 2017. Glacier mass loss during the 1960s and 1970s in the Ak-Shirak range (Kyrgyzstan) from multiple stereoscopic Corona and Hexagon imagery. Rem. Sens. 9 (3), 275−292. https://doi.org/10.3390/rs9030275.

Guo, L., Li, J., Li, Z., et al., 2020. The surge of the Hispar Glacier, Central Karakoram: SAR 3-D flow velocity time series and thickness changes. J. Geophys. Res. Solid Earth 125. https://doi.org/10.1029/2019JB018945.

Haemmig, C., Huss, M., Keusen, H., et al., 2014. Hazard assessment of glacial lake outburst floods from Kyagar glacier, Karakoram mountains, China. Ann. Glaciol. 55, 34−44. https://doi.org/10.3189/2014AoG66A001.

Heid, T., Kääb, A., 2012. Repeat optical satellite images reveal widespread and long term decrease in land-terminating glacier speeds. Cryosphere 6, 467−478. https://doi.org/10.5194/tc-6-467-2012.

Hoinkes, H.C., 1969. Surges of the Vernagtferner in the Ötztal Alps since 1599. Can. J. Earth Sci. 6, 853. https://doi.org/10.1139/e69-086.

Huss, M., 2013. Density assumptions for converting geodetic glacier volume change to mass change. Cryosphere 7, 877−887. https://doi: 10.5194/tc-7-877-2013.

Huss, M., Bauder, A., Funk, M., 2009. Homogenization of long-term mass-balance time series. Ann. Glaciol. 50 (50), 198−206. https://doi: 10.3189/172756409787769627.

Jenkins, M., Kaspari, S., Kang, S.-C., et al., 2016. Tibetan Plateau Geladaindong black carbon ice core record (1843−1982): recent increases due to higher emissions and lower snow accumulation. Adv. Clim. Change Res. 7, 132−138. https://doi.org/10.1016/j.accre.2016.07.002.

Jiang, S., Yang, T., Tian, H., 2012. Glacier shrinkage and its dependence on climate in the Malan mountain in past 40 years based on RS and GIS. J. Glaciol. Geocryol. 34 (3), 522−529 (Chinese).

Jiskoot, H., 2011. Glacier surging. In: Encyclopedia of Snow, Ice and Glaciers. Springer, Dordrecht.

Kääb, A., Treichler, D., Nuth, C., et al., 2015. Brief communication: contending estimates of 2003−2008 glacier mass balance over the Pamir−Karakoram−Himalaya. Cryosphere 9, 557−564. https://doi.org/10.5194/tc-9-557-2015.

Kääb, A., Leinss, S., Gilbert, A., et al., 2018. Massive collapse of two glaciers in western Tibet in 2016 after surge-like instability. Nat. Geosci. 11, 114−120. https://doi.org/10.1038/s41561-017-0039-7.

King, O., Bhattacharya, A., Bhambri, R., et al., 2019. Glacial lakes exacerbate Himalayan glacier mass loss. Sci. Rep. 9, 18145. https://doi.org/10.1038/s41598-019-53733-x.

Kochtitzky, W., Winski, D., McConnell, E., et al., 2020. Climate and surging of Donjek glacier, Yukon, Canada. Arctic Antarct. Alpine Res. 52 (1), 264−280. https://doi:10.1080/15230430.2020.1744397.

Liu, L., Jiang, L., Jiang, H., et al., 2019. Accelerated glacier mass loss (2011−2016) over the Puruogangri ice field in the inner Tibetan Plateau revealed by bistatic InSAR measurements. Remote Sens. Environ. 231, 111241. https://doi.org/10.1016/j.rse.2019.111241.

Lv, M., Guo, H., Lu, X., et al., 2019. Characterizing the behaviour of surge- and non-surge-type glaciers in the Kingata Mountains, eastern Pamir, from 1999 to 2016. Cryosphere 13 (1), 219−236. https://doi: 10.5194/tc-13-219-2019.

McNabb, R., Nuth, C., Kääb, A., et al., 2019. Sensitivity of glacier volume change estimation to DEM void interpolation. Cryosphere 13, 895−910. https://doi: 10.5194/tc-13-895-2019.

Mölg, T., Maussion, F., Scherer, D., 2014. Mid-latitude westerlies as a driver of glacier variability in monsoonal High Asia. Nat. Clim. Change 4, 68−73. https://doi.org/10.1038/NCLIMATE2055.

Mukherjee, K., Bolch, T., Goerlich, F., et al., 2017. Surge-type glaciers in the tien Shan (central Asia). Arctic Antarct. Alpine Res. 49, 147−217. https://doi: 10.1657/AAAR0016-021.

Neckel, N., Kropácek, J., Bolch, T., et al., 2014. Glacier mass changes on the Tibetan Plateau 2003−2009 derived from ICESat laser altimetry measurements. Environ. Res. Lett. 9 (1), 014009. https://doi: 10.1088/1748-9326/9/1/014009.

Nuth, C., Kääb, A., 2011. Co-registration and bias corrections of satellite elevation data sets for quantifying glacier thickness change. Cryosphere 5, 271−290. https://doi: 10.5194/tc-5-271-2011.

Paul, F., 2015. Revealing glacier flow and surge dynamics from animated satellite image sequences: examples from the Karakoram. Cryosphere 9, 2201−2214. https://doi.org/10.5194/tc-9-2201-2015.

Paul, F., 2019. Repeat glacier collapses and surges in the Amney Machen Mountain Range, Tibet, possibly triggered by a developing Rock-Slope instability. Rem. Sens. 11, 708. https://doi.org/10.3390/rs11060708.

Paul, F., Barrand, N.E., Berthier, E., et al., 2013. On the accuracy of glacier outlines derived from remote sensing data. Ann. Glaciol. 54, 171−182. https://doi:10.3189/2013AoG63A296.

Pieczonka, T., Bolch, T., 2015. Region-wide glacier mass budgets and area changes for the Central Tien Shan between ~1975 and 1999 using Hexagon KH-9 imagery. Global Planet. Change 128, 1−13. https://doi: 10.1016/j.gloplacha.2014.11.014.

Pieczonka, T., Bolch, T., Wei, J.F., et al., 2013. Heterogenous mass loss of glaciers in the Aksu-Tarim catchment (Central Tien Shan) revealed by 1976 KH-9 Hexagon and 2009 SPOT-5 stereo imagery. Rem. Sens. Environ. 130, 233−244. https://doi.org/10.1016/j.rse.2012.11.020.

Quincey, D.J., Glasser, N.F., Cook, S.J., Luckman, A., 2015. Heterogeneity in Karakoram glacier surges. J. Geophys. Res. Earth Surf. 120 (7), 1288−1300. https://doi.org/10.1002/2015JF003515.

Quincey, D.J., Braun, M., Glasser, N.F., et al., 2011. Karakoram glacier surge dynamics. Geophys. Res. Lett. 38 (18) https://doi.org/10.1029/2011GL049004.

RGI Consortium, 2017. Randolph Glacier Inventory: a dataset of global glacier outlines. https://doi.org/10.7265/N5-RGI-60, version 6.0.

Rolstad, C., Haug, T., Denby, B., 2009. Spatially integrated geodetic glacier mass balance and its uncertainty based on geostatistical analysis: application to the western Svartisen ice cap, Norway. J. Glaciol. 55, 666−680. https://doi:10.3189/002214309789470950.

Sakai, A., Fujita, K., 2017. Contrasting glacier responses to recent climate change in high-mountain Asia. Sci. Rep. 7 (1), 13717. https://doi.org/10.1038/s41598-017-14256-5.

Sakai, A., Nuimura, T., Fujita, K., et al., 2015. Climate regime of Asian glaciers revealed by GAMDAM glacier inventory. Cryosphere 9 (3), 865−880. https://doi.org/10.5194/tc-9-865-2015.

Sevestre, H., Benn, D.I., 2015. Climatic and geometric controls on the global distribution of surge-type glaciers: implications for a unifying model of surging. J. Glaciol. 61 (228), 646−662. https://doi: 10.3189/2015JoG14J136.

Shean, D.E., Alexandrov, O., Moratto, Z.M., et al., 2016. An automated, open-source pipeline for mass production of digital elevation models (DEMs) from very-high-resolution commercial stereo satellite imagery. ISPRS J. Photogramm. 116, 101−117. https://doi.org/10.1016/j.isprsjprs.2016.03.012.

Shean, D.E., Bhushan, S., Montesano, P., et al., 2020. A systematic, regional assessment of High-Mountain Asia glacier mass balance. Front. Earth Sci. 7, 331. https://doi: 10.3389/feart.2019.00363.

Shi, Y., Hsieh, T.-C., Chen, P.-H., et al., 1980. Distribution, Features and Variation of Glaciers in China, vol. 126. IAHS Publication, Wallingford, pp. 111−116.

Sund, M., Eiken, T., Hagen, J.O., et al., 2009. Svalbard surge dynamics derived from geometric changes. Ann. Glaciol. 50, 50−60. https://doi: 10.3189/172756409789624265.

Thøgersen, K., Gilbert, A., Schuler, T.V., et al., 2019. Rate-and-state friction explains glacier surge propagation. Nat. Commun. 10, 2823. https://doi.org/10.1038/s41467-019-10506-4.

Vijay, S., Braun, M.H., 2016. Elevation change rates of glaciers in the Lahaul-Spiti (western Himalaya, India) during 2000−2012 and 2012−2013. Rem. Sens. 8 (12), 1038. https://doi.org/10.3390/rs8121038.

Wu, K., Liu, S., Jiang, Z., et al., 2018. Recent glacier mass balance and area changes in the Kangri Karpo Mountains from DEMs and glacier inventories. Cryosphere 12, 103−121. https://doi.org/10.5194/tc-12-103-2018.

Xu, J., Shangguan, D., Wang, J., 2018. Three-dimensional glacier changes in geladandong peak region in the central Tibetan Plateau. Water 10, 1749. https://doi.org/10.3390/w10121749.

Xu, J., Liu, S., Zhang, S., Guo, W., Wang, J., et al., 2013. Recent changes in glacier area and volume on Tuanjiefeng peak region of Qilian Mountains, China. PloS One 8 (8), e70574. https://doi:10.1371/journal.pone.0070574.

Yao, T., Thompson, L., Yang, W., et al., 2012. Different glacier status with atmospheric circulations in Tibetan Plateau and surroundings. Nat. Clim. Change 2, 663−667. https://doi.org/10.1038/nclimate1580.

Yasuda, T., Furuya, M., 2015. Dynamics of surge-type glaciers in West Kunlun Shan, Northwestern tibet. J Geophys. Res. Earth 120, 2393−2405. https://doi.org/10.1002/2015JF003511.

Yde, J.C., Knudsen, N.T., 2007. 20th-century glacier fluctuations on Disko island (Qeqertarsuaq), Greenland. Ann. Glaciol. 46, 209−214. https://doi.org/10.3189/172756407782871558.

Zhang, Y., Kang, S., Grigholm, B., et al., 2016. Twentieth-century warming preserved in a Geladaindong Mountain ice core, central Tibetan Plateau. Ann. Glaciol. 57, 70−80. https://doi.org/10.3189/2016AoG71A001.

Zhang, Z., Liu, S., Zhang, Y., et al., 2018. Glacier variations at Aru Co in western Tibet from 1971 to 2016 derived from remote-sensing data. J. Glaciol. 64 (245), 397−406. https://doi: 10.1017/jog.2018.34.

Zhang, Z., Du, Z., Liu, S., et al., 2020. glacier mass changes over Duxueshan, Burog Kangri, and Zangser Kangri in the inner Tibetan Plateau. Environ. Earth. Sci. 79, 292. https://doi.org/10.1007/s12665-020-09044-w.

Zhou, Y., Li, Z., Li, J., et al., 2018. Glacier mass balance in the Qinghai−Tibet Plateau and its surroundings from the mid-1970s to 2000 based on Hexagon KH-9 and SRTM DEMs. Rem. Sens. Environ. 210, 96−112. https://doi.org/10.1016/j.rse.2018.03.020, 2018.